130 KSME Journal, Vol. 3, No. 2, pp. 130~138, 1989.

CONTACT ANALYSIS OF NONLINEAR SHELL STRUCTURES USING A MATHEMATICAL PROGRAMMING METHOD

Gyu Bong Lee*, Young Gon Kim* and Byung Man Kwak**

(Received July 24, 1989)

In the present study a shell contact problem with geometric and material nonlinearities is efficiently formulated by utilizing the mathematical programming method. The contact surface is assumed unbonded and frictionless. An incremental analysis by the updated Lagrangian approach is used. Two representative problems are treated to show modeling of the shell contact and the proposed solution method. The results are compared with existing solutions and those calculated by a commerical package.

Key Words: Geometric Nolinearity, Updated Lagrangian Approach, Quadratic Programming Method, Isoparametric Degenerate Nine-Node Shell Element

1. INTRODUCTION

The contact processes often encountered in many practical engineering field problems cause stress concentration at or near the surface of contact and eventually lead to a failure of one or both of the mating bodies. Therefore, the understanding of exact contact area and pressure distribution between the bodies has been a matter of interest and importance for a long time. However, it is very difficult to obtain accurate solutions of the contact problems due to their inherent characteristic that the boundary conditions of the bodies under consideration are not known prior to the analysis, but they depend on the solution.

The so called mathematical programming method is well developed for the analysis of linear elastic contact problems where the finite element technique is often used. They are formulated either by minimizing the potential energy with certain kinematic constraints along contact surfaces or as a variational inequality. Solutions are then obtained by using a quadratic programming method(Hung, 1980), sequential linear programming method(Haug, 1978), or penalty method(Oden, 1984). Most recently, the methods have been extended to solve small(Kikuchi, 1981) or large(Cheng, 1985 and Joo, 1986) deformation elasto-plastic contact problems.

The works cited above deal with two dimensional continuum contact problems. In contrast to the extensive studies of those contact problems, however, only limited attention has been given to beam, plate, and shell structural contact problems. In Chaudhary(1986) a contact constraint equation for a class of nonlinear three dimensional contact problems was incorporated to the global equation by the Lagrangian multiplier technique. A quadratic programming method was implemented for the analysis of two dimensional elastic beam contact problems under large displacement in Lee(1989).

On the other hand, a nonlinear shell theory was employed to analyze the axisymmetric behavior of an elastic spherical shell compressed by smooth rigid plates in Updike(1972). In Tielking(1981) a discrete Fourier transform technique was presented for obtaining the influence coefficient matrix for a toroidal shell contact analysis.

In the present paper, a shell contact problem with geometric and material nonlinearities is dealt with through the extension of the solution method presented in Lee(1989). Based on a general continuum mechanics theory, governing equations of generally nonlinear contact problems are presented in an incremental form through adoption of the updated Lagrangian approach. Thus, arbitrarily large displacements and rotations are admitted with elasto-plastic deformation involved. However, the strain is assumed small, which means that the thickness of a shell is not updated but kept constant.

A geometric compatibility condition in the potential contact region is described by using the geometric representations of the potential contact surfaces. The contact surface is assumed unbonded and frictionless. Contact between two bodies is checked not on the mid-surface of a shell as often done in the literature but on the upper or lower surface in order not to neglect the shell thickness. Potential contact check points located on the potential contact surface are proposed for more accurate representation of this phenomenon. Two numerical examples are treated for validation of the formulation and solution method presented in this paper.

2. INCREMENTAL FORMULATION OF THE PROBLEM

In this section, in parallel to Lee(1989), governing equations for a class of contact problems including geometric and material nonlinearities are described in an incremental form through adoption of the updated Lagrangian approach. In the incremental approach, knowing the solution up to a discrete

*Mechanical Systems Lab., Korea Institute of Science and Technology, P.O. Box 131, Cheongryang, Seoul 130-650, Korea.
**Department of Mechanical Engineering, Korea Advanced Institute of Science and Technology, P.O. Box 150, Cheongryang, Seoul 130-650, Korea.

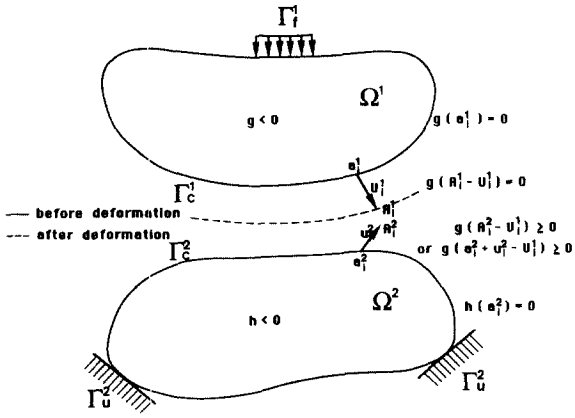

Fig. 1 Schematic representation of contact problem

time or a loading parameter t, the solution for the discrete time $t+\Delta t$ is sought, where Δt is a suitably chosen time increment. The descriptions in this section are basically the same as those in Lee (1989), but summarized for introduction of notation and completeness.

Denoting the coordinates of a generic point in a body at time t and time $t+\Delta t$ as a_i and x_i, respectively, we can define the increments in the displacements from time t to time $t+\Delta t$ as

$$u_i = x_i - a_i \tag{1}$$

Firstly, two body contact problems are considered for the description of the equations and solution approaches without loss of generality. In the present paper, however, the simpler contact problems between one flexible body and one rigid body are chosen as numerical examples, which is only due to the easiness and brevity in the geometric representations of the potential contact surfaces. Thus, the description will be specialized for the simpler problems in the later section.

As shown in Fig. 1, the region occupied by each body under consideration and its boundary surface are denoted as Ω and Γ, respectively. The boundary surface Γ is composed of three disjoined parts: Γ_u on which displacements are prescribed, Γ_f on which tractions are prescribed, and a potential contact surface region Γ_c.

The contact pressure p at time $t+\Delta t$ is defined on Γ_c as

$$p = -{}^{t+\Delta t}\sigma_{ij}\,{}^{t+\Delta t}n_j\,{}^{t+\Delta t}n_i \tag{2}$$

where ${}^{t+\Delta t}\sigma_{ij}$ and ${}^{t+\Delta t}n_i$ represent the Cauchy stress tensor and the unit outer normal vector at time $t+\Delta t$, respectively. The usual summation convention is used here. Under the assumption of unbonded contact problem, the pressure must be nonnegative, that is,

$$p \geq 0 \tag{3}$$

One of the two bodies, called body 1 hereafter, is assumed to have rigid body motions. Then the global equilibrium of body 1 is expressed as

$$\int_{t+\Delta t\Gamma_f^1} {}^{t+\Delta t}f_i\beta_{ij}\,{}^{t+\Delta t}d\Gamma = \int_{t+\Delta t\Gamma_c^1} p\alpha_{ij}\,{}^{t+\Delta t}n_i\,{}^{1\ t+\Delta t}d\Gamma \tag{4}$$

where the coefficients α_{ij} and β_{ij} represent the rigid body displacements of points on Γ_c^1 and Γ_f^1, respectively, in the i-th coordinate direction due to a unit displacement in the j-th rigid body degree of freedom. ${}^{t+\Delta t}f_i$ denotes the traction vector at time $t+\Delta t$ defined as

$${}^{t+\Delta t}f_i = {}^{t+\Delta t}\sigma_{ij}\,{}^{t+\Delta t}n_j \text{ on } \Gamma_f^m \tag{5}$$

A right superscript m is used to designate quantities associated with the m-th body. For simplicity, no body force is considered in *Eq.*(4) and friction is assumed negligible.

The equation of internal equilibrium of each body is expressed as (Fung, 1965)

$$({}^{t+\Delta t}S_{jk}x_{i,k})_{,j} = 0 \qquad \text{in } \Omega^m \tag{6}$$

where ${}^{t+\Delta t}S_{ij}$ represents the 2nd Piola-Kirchhoff stress tensor corresponding to the configuration at time $t+\Delta t$ but measured in the configuration at time t. The notation $(\ )_{,j}$ denotes differentiation with respect to the coordinate a_j. The stress-strain constitutive relation is given as

$$dS_{ij} = C_{ijrs}\varepsilon_{rs} \tag{7}$$

where dS_{ij} represents the 2nd Piola-Kirchhoff stress increment components, C_{ijrs} the elasto-plastic constitutive coefficient at current time t, and ε_{ij} the Lagrangian strain components defined as

$$\varepsilon_{ij} = e_{ij} + \eta_{ij} \tag{8}$$

where

$$e_{ij} = \frac{1}{2}(u_{i,j} + u_{j,i}) \text{ and } \eta_{ij} = \frac{1}{2}u_{k,i}\,u_{k,j}$$

Displacement boundary conditions for body 2 are given as

$$u_i = 0 \text{ on } \Gamma_u^2 \tag{9}$$

As shown in Fig. 1, let the geometries of potential contact surfaces at time t be described by smooth functions,

$$g(a_i^1) = 0, \quad h(a_i^2) = 0 \tag{10}$$

The impenetration condition that no material particle will penetrate into the surface of the opposing body can then be expressed at time $t+\Delta t$(Lee, 1988 and Kwak, 1989)

$$D_n(a_i^1) = g(a_i^2 + u_i^2 + U_i^1) \geq 0 \quad \text{for all } a_i^1 \text{ on } \Gamma_c^1 \tag{11}$$

where

$$U_i^1 = u_i^1 + \alpha_{ij}\,q_j$$

and q_j denotes the rigid body displacement increments of body 1 from time t to time $t+\Delta t$. In addition to the conditions (3) and (11), the following geometric compatibility condition must also be satisfied at time $t+\Delta t$

$$p \cdot D_n(a_i^1) = 0 \text{ for all } a_i^1 \text{ on } \Gamma_c^1 \tag{12}$$

This states that either the contact force or the gap between two contacting bodies must be equal to zero.

The governing equation for frictionless contact is now completed. It is known that an equivalent minimization problem suitable for a numerical analysis exists as follows:

$$\min J_1(u, q) \tag{13}$$

$$\text{subject to } D_n(a_i^1) \geq 0 \text{ on } \Gamma_c^1 \tag{14}$$

where

$$J_1(u, q) = \sum_{m=1}^{2}\left[\int_{t_\Omega m}\left({}^t\sigma_{ij} + \frac{1}{2}\, dS_{ij}\right)\varepsilon_{ij}\, {}^t d\Omega\right] - \int_{t+\Delta t\Gamma_f m}^{t+\Delta t} f_i\, u_i\, {}^{t+\Delta t}d\Gamma - \int_{t+\Delta t\Gamma_f^1}^{t+\Delta t} f_i \beta_{ij}\, q_{ij}\, {}^{t+\Delta t}d\Gamma$$

The equivalence of this minimization problem to the governing equations described previously has been shown in detail by Joo(1986). It is noted that the contact pressure p corresponds to the Lagrange multiplier corresponding to the constraint(14).

3. IMPLEMENTATION OF MATHEMATICAL PROGRAMMING METHOD

As in our previous papers, a quadratic programming method is implemented to solve the minimization problem defined above. That is, the highly nonlinear minimization problem is treated by a sequence of quadratic programming problems through the following approximations and subsequent uqdating to be described later,

$$C_{ijrs}\, \varepsilon_{ij}\, \varepsilon_{rs} \cong C_{ijrs}\, e_{ij}\, e_{rs} \tag{15}$$

$$g(a_i^2 + u_i^2 - U_i^1) \cong g(a_i^2) + (u_k^2 - U_k^1)\, \dot{g}_k(a_i) \tag{16}$$

where

$$\dot{g}_k(a_i) = \frac{\partial g(a_i)}{\partial a_k}\bigg|_{a_i = a_i^2}$$

Now we have the approximated impenetration condition instead of the condition (11):

$$-u_k^1 \dot{g}_k(a_i) + u_k^2 \dot{g}_k(a_i) - \alpha_{kj} q_j \dot{g}_k(a_i) + g(a_i^2) \geq 0 \text{ on } \Gamma_c^1 \tag{17}$$

It is natural that there exist the errors due to the approximations (15) and (16). The errors can be small for a load increment but accumulated leading to gross errors or instability of the solution. The accumulation of the solution errors can be particularly serious in elasto-plastic analysis. Therefore, an equilibrium iteration is very desirable at all load steps.

In the present study the calculated solutions are improved through the Newton-Raphson iterative solution scheme for every load increment step. If we denote the vector of the nodal displacement increment of discretized bodies as u in order to follow the usual finite element procedure, the vector $u^{(i)}$ after the i-th sub-iteration is obtained as follows:

$$u^{(i)} = u^{(i-1)} + \Delta u \tag{18}$$

where Δu denotes the nodal displacement change at the i-th sub-iteration.

Substituting Eq.(17) into Eq.(14) and considering Eq.(18), we have the discretized quadratic programming problem for a sub-iteration as

$$\min J_2(\Delta u, \Delta q) \tag{19}$$

$$\text{subject to } \sum_{m=1}^{2} M^m\, \Delta u^m + A\, \Delta q - d \leq 0 \tag{20}$$

where

$$J_2(\Delta u, \Delta q) = \sum_{m=1}^{2}\left[\frac{1}{2}(\Delta u^m)^T K^m \Delta u^m - (F^m)^T \Delta u^m\right] - (F_e^1)^T H\, \Delta q$$

with

$$K = \int_{t_\Omega} (B_L^T C B_L + B_{NL}^T \tau B_{NL})\, {}^t d\Omega$$

$$F = F_e - F_t$$

$$F_e = \int_{t+\Delta t\Gamma_f}^{t+\Delta t} f_i^{t+\Delta t} d\Gamma$$

$$F_t = \int_{t_\Omega} B_L^{Tt}\, \hat{\tau}\, {}^t d\Omega$$

In the above equations, Δq is the vector of rigid body displacement change at the i-th sub-iteration, H is a kinematic transformation matrix that gives the rigid body displacements at the points where external loads are applied, and the following notation is also used for the calculation of the element matrices:

B_L, B_{NL} = linear and nonlinear strain-displacement matrices

C = incremental stress-strain material property matrix

${}^t\tau, {}^t\hat{\tau}$ = matrix and vector of Cauchy stresses

The stiffness matrix K and the force vector F_t are updated every iteration by using $u^{(i)}$ obtained by Eq.(18).

Matrices A and M, and vector d designating the geometric compatibility condition are obtained from the approximated constraint condition (17) (see APPENDIX). They should be recalculated every iteration since the geometry of potential contact surface of each body may change in succession.

In the special case that body 1 is rigid body as to be dealt with in the numerical examples, Eqs.(19) and (20) are reduced to the quadratic programming problem defined as

$$\min J_3(\Delta u, \Delta q) \tag{21}$$

$$\text{subject to } M^2\, \Delta u^2 + A\, \Delta q - d \leq 0 \tag{22}$$

where

$$J_3(\Delta u, \Delta q) = \frac{1}{2}(\Delta u^2)^T K^2\, \Delta u^2 - (F^2)^T \Delta u^2 - (F_e^1)^T H \Delta q$$

Equations (21) and (22) state that the discretized contact problem becomes as quadratic programming problem with

design variables Δu and Δq. Since the number of design variables of this problem is usually larger than that of constraints, the dual problem is more efficient(Lee 1989). In this case, it can be shown in Joo(1986) that the dual variables actually denote the constraining forces to impose the impenetration constraints. From the forces, the contact pressure can be determined as to be explained in the examples. However, this does not mean that the shell element implemented on the basis of the displacement finite element method as shown in the next section can accept element surface forces.

4. CONSIDERATIONS FOR APPLICATION TO SHELL CONTACT PROBLEMS

The isoparametric degenerate nine-node shell elements as shown in Fig. 2 are employed to discretize shell structures under consideration. The formulation of the shell element is shown on the basis of the general continuum mechanics in Bathe(1980). The basic kinematic assumption considered for the formulation is that lines originally normal to the shell mid-surface remain straight during deformation, but the lines are not necessarily normal to the deformed mid surface due to transverse shear deformations, and that the transverse normal stress is zero. Arbitrarily large displacements and rotations are allowed in the element. However, strain is still assumed small, which means that the thickness of a shell is not updated but kept constant.

In discretizing the condition (17), a finite number of points from the matching surfaces are selected. In general these potential contact check points can be chosen arbitrarily, not considering matching. The element nodes are located on the mid-surface of shell, but the potential contact check points located on the upper or lower surface of the shell due to the thickness. The number of the contact check points in a shell element can be chosen differently from that of the nodes.

The locations $\tilde{a}_i$ of the potential contact check points are defined at the start in terms of the natural coordinates ξ, η and ζ and n nodal point coordinates, a_i, $k=1, \cdots, n$;

$$\tilde{a}_i = \sum_{k=1}^{n} N_k \left(a_i^k + \frac{\zeta}{2} h_k {}^t V_{ni}^k \right) \tag{23}$$

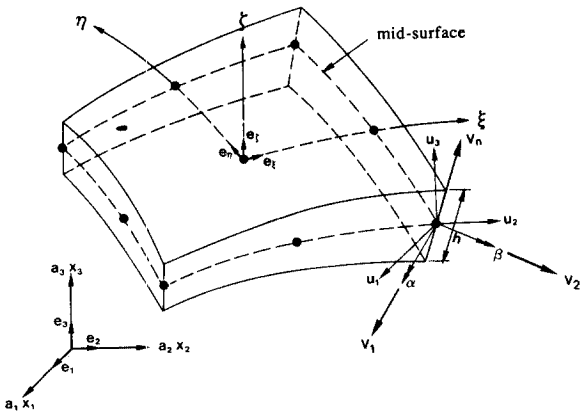

Fig. 2 Isoparametric degenerate nine-node shell element

where the $N_k(\xi, \eta)$ are the interpolation functions, h_k is the thickness of shell in ζ direction at nodal point k, and the value of ζ is always equal to 1 or -1. ${}^t V_{ni}$ denotes the components of unit vector ${}^t V_n$ normal to the shell mid-surface in direction ζ at nodal point k at time t.

The elasto-plastic constitutive coefficient C_{ijrs} of Eq.(7) is given as (Nagtegaal, 1981)

$$C_{ijrs} \cong D_{ijrs} - \frac{1}{2}({}^t\sigma_{ir}\delta_{js} + {}^t\sigma_{is}\delta_{jr} + {}^t\sigma_{jr}\delta_{is} + {}^t\sigma_{js}\delta_{ir}) \tag{24}$$

where the moduli D_{ijrs} was derived by Yamada (1967) for the elasto-plastic material behavior according to the Prandtl-Reuss relation, the von Mises yield condition, and the isotropic work-hardening.

However, the basic assumption must be considered that no transverse normal stress is developed. Thus, the moduli to be employed in the shell element formulation is obtained as

$$C_{ijrs} \cong D'_{ijrs} - \frac{1}{2}({}^t\sigma_{ir}\delta_{js} + {}^t\sigma_{is}\delta_{jr} + {}^t\sigma_{jr}\delta_{is} + {}^t\sigma_{js}\delta_{ir}) \tag{25}$$

where

$$D'_{ijrs} = D_{ijrs} - D_{ij33}\frac{D_{33rs}}{D_{3333}}$$

In Eq.(25) it is also necessary that a shear correction factor be appended to take into account of the non-uniformity of the shearing strains γ_{23} and γ_{31} over the cross section of shell.

The following matrix form of the constitutive relation is obtained when the 2nd Piola-Kirchhoff stress increment vector ΔS and the Lagrange strain vector ε store global Cartesian components :

$$\Delta \hat{S} = T_\varepsilon{}^T C T_\varepsilon \varepsilon \tag{26}$$

where

$$\Delta \hat{S} = [\Delta S_1 \quad \Delta S_2 \quad \Delta S_3 \quad \Delta S_{12} \quad \Delta S_{23} \quad \Delta S_{31}]^T$$
$$\varepsilon = [\varepsilon_1 \quad \varepsilon_2 \quad \varepsilon_3 \quad \gamma_{12} \quad \gamma_{23} \quad \gamma_{31}]^T$$

and C is the stress-strain matrix corresponding to the moduli C_{ijrs} of Eq.(25). The transformation matrix T_ε is different from location to location and has to be evaluated for all integration points every iteration.

In the present study the reduced 2×2 Gauss integration scheme, one of the most popular schemes proposed to alleviate the element locking effects, is adopted for numerical integration procedures over the shell surfaces. In order to suppress the possible spurious zero energy modes, arbitrarily small stiffness coefficient matrix may be added to the stiffness matrix evaluated by the reduced integration scheme. The Newton-Cotes integration scheme is employed for numerical integration procedures through the shell thickness. The onset and spread of the plastic conditions through the element thickness can be captured effectively by this selection.

5. NUMERICAL EXAMPLES

A computer program has been developed to solve elasto-plastic shell contact problems under large displacement based

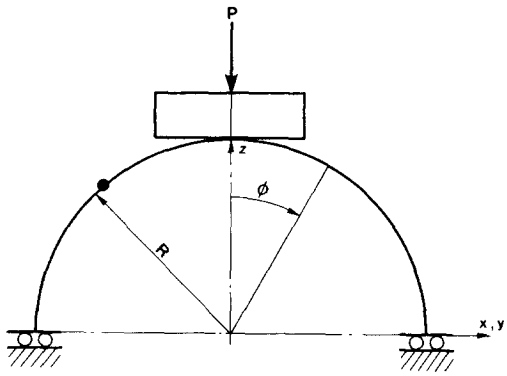

Fig. 3 Hemispherical shell compressed by a flat rigid plate

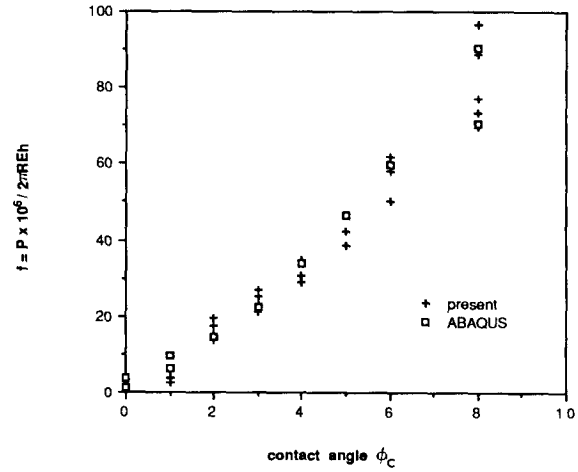

Fig. 5 Load versus contact angle ϕ_c for elastic shell

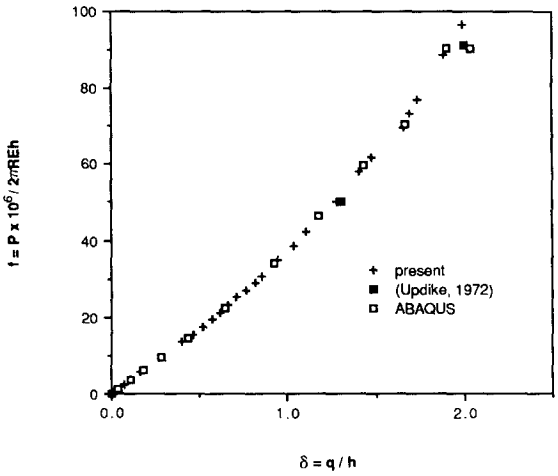

Fig. 4 Load versus plate displacement for elastic shell

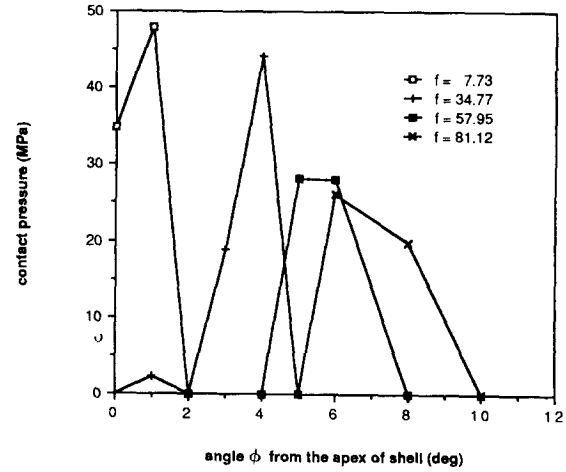

Fig. 6 Distribution of contact pressure for elastic shell

on the above proposed formulation. For the elasto-plastic analysis we used the basic solution procedure as summarized in Bathe (1982) with the constitutive relation and the seven point Newton-Cotes integration formula as previously mentioned. Two representative practical examples are presented. Due to symmetry only a quarter of each body was modeled by 38 nine-node shell elements. They were run on an CRAY-2S supercomputer in the authors' institute.

(1) Hemispherical Shell Compressed By a Rigid Plate

A hemispherical shell compressed by a flat rigid plate as shown in Fig. 3 is treated as the first numerical example. Although this problem can be modeled as an axisymmetric case, for the purpose of treating a general shell element one quarter of the shell is modeled as mentioned earlier. Material properties of the shell having a radius of $R=200$mm and a thickness of $h=2$mm are assumed; $E=206$GPa and $\nu=0.3$. The material is also assumed perfectly plastic with a yield stress of $\sigma_y=296$MPa.

When the deformation of the shell is begun, the deformed shell consists of a contact region and a free region, and the contact region lies nearly flat against the rigid plate. The angle between the axis of symmetry and the normal of undeformed shell is denoted as ϕ as shown in Fig. 3, and the value of ϕ to the boundary of the contact region as ϕ_c.

The results obtained through a purely elastic analysis are first presented. Figure 4 shows the load versus plate displacement relations. Here two nondimensional parameters, $f=P\times10^6/2\pi$REh and $\delta=q/h$, are employed.

In Updike(1972), the problem was assumed axisymmetric and a nonlinear shell theory was employed for the analytic solution. That is, the solution was obtained by assuming a value of ϕ_c and solving the boundary-value problem on the assumption that the contact region $\phi<\phi_c$ remains flat. They also showed that a bifurcation occurs, namely, the shell buckles into a dimple shape away from the rigid constraining plate at $\phi_c=8.1$ degree.

This problem has also been analyzed by using the ABAQUS program. For the ABAQUS run, a half of the shell section is modeled by ten axisymmetric three node shell elements since it is very difficult to treat three-dimensional shell contact problems using the program. As shown in Fig. 4, they all agree well, except the disagreement between the present and the other solutions above the load level $f=90$. It is conjectured that a bifurcation starts around this point, but the present algorithm is not meant for this region.

The variation of contact angle ϕ_c against increasing external load is displayed in Fig. 5. Due to the discrete nature of potential contact check points and finite size of the elements,

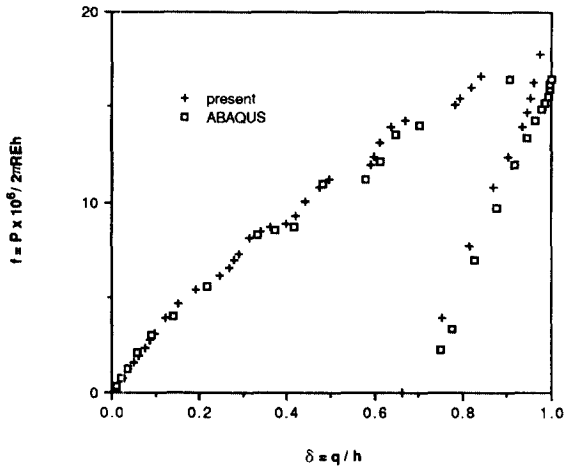

Fig. 7 Load versus plate displacement for elasto-plastic shell

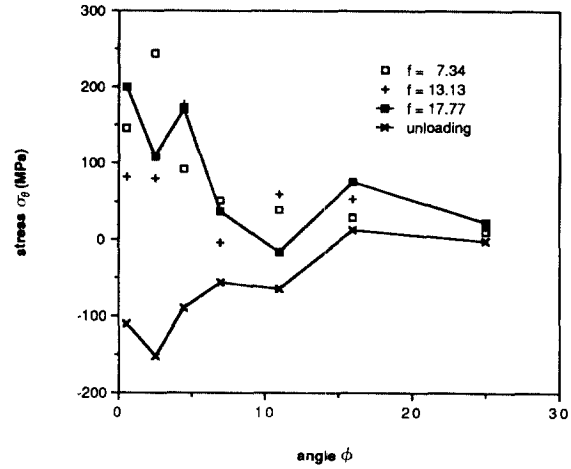

(a) outer surface

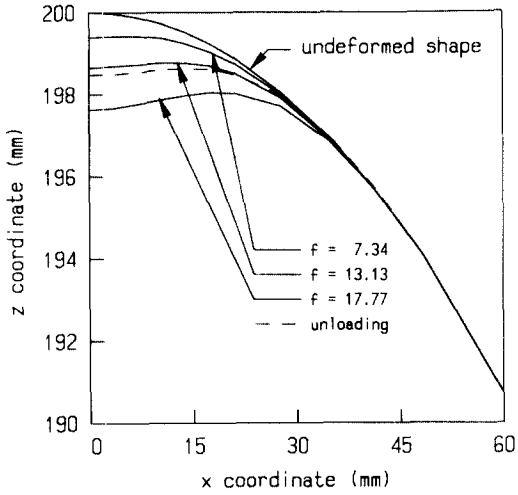

Fig. 8 Deformed shapes of elasto-plastic shell

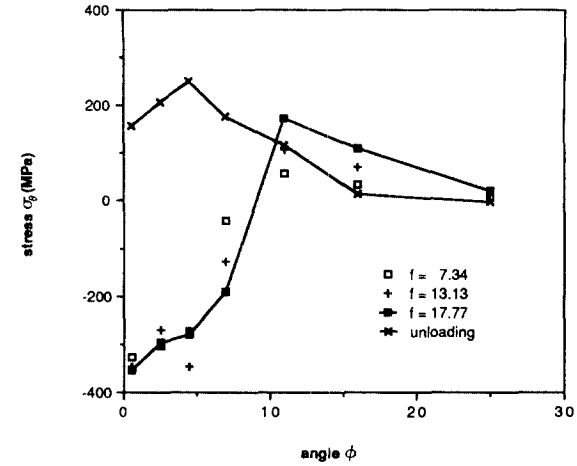

(b) inner surface

Fig. 9 Circumferential stress σ_θ along ϕ for elasto-plastic shell

the variation appears intermittent. Figure 6 shows the distributions of contact pressure. They were obtained by dividing the contact forces at the contact points by their surrounding areas and taking the mean of them according to the angle ϕ. This figure exhibits that some previously contacted points near the apex of shell were separated and contact took place at new check points of larger ϕ_c for higher load levels. The region $\phi < \phi_c$ did not remain flat any longer above some load level. A small dimple might be formed inside the contact region, though it did not incur a global buckling.

Next an elasto-plastic analysis is performed. Figure 7 shows the load versus plate displacement relations. Generally, little discrepancy is shown between the present results and the results obtained from the ABAQUS run. It is presumed that the disagreements between two numerical results at some load levels were due to the abrupt change of contact angle ϕ_c and the difference of the two element models.

The loading for the present results is continued until the value of f reaches 17.77, which is taken arbitrarily. The applied load is then reduced to zero. The first yielding occurs at $f=1.55$ for the outer surface and at $f=1.93$ for the inner surface. The elastic springback in the plate displacement due to the unloading is 32% of the maximum value. The deformed shapes of the mid-surface of the shell for various load levels are displayed in Fig. 8. The contact pressure at the center becomes zero when f reaches about 13.

Figure 9 and 10 show variations of the circumferential stress σ_θ and the effective stress $\bar{\sigma}$ along the meridian angle ϕ on the inner and outer surfaces for various load levels. The stress distributions often show wide variations, indicating the complex nature of the machanics in addition to the finiteness in the discretization procedure.

In the present study the residual stresses can be obtained easily since the same solution procedures have been employed for loading and unloading. Expectedly, the outer surface near the apex of shell has tensile residual stress while the inner surface has compression. Very small portions seem to remain plastic even after complete unloading as shown in Fig. 10.

(2) Clamped Square Plate Stretched by a Rigid Punch

As a second example a clamped square plate stretched by a hemispherical rigid punch has been considered. The geometry of the problem is given in Fig. 11, where the radius of bottom surface of the punch is denoted as R. The plate with

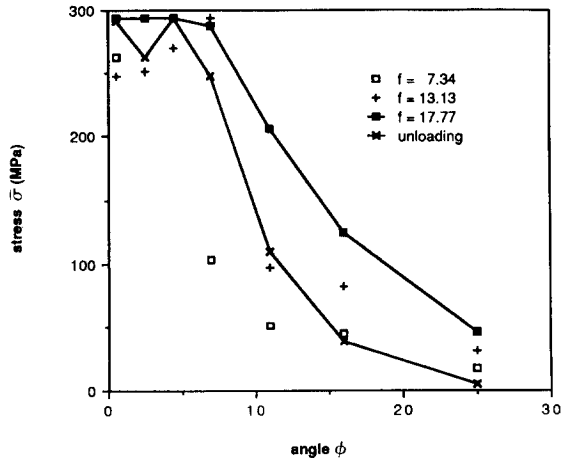

(a) outer surface

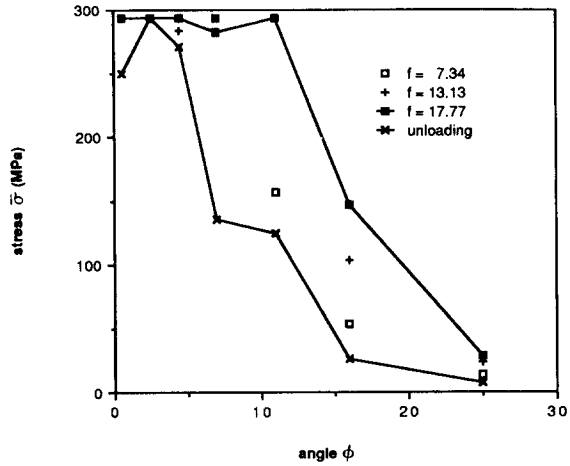

(b) inner surface

Fig. 10 Effective stress $\bar{\sigma}$ along ϕ for elasto-plastic shell

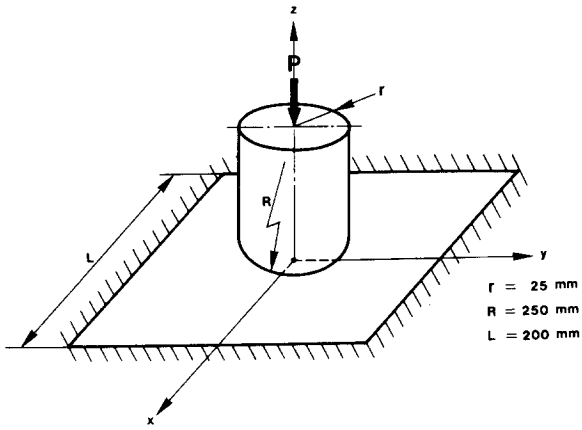

Fig. 11 Clamped square plate stretched by a rigid punch

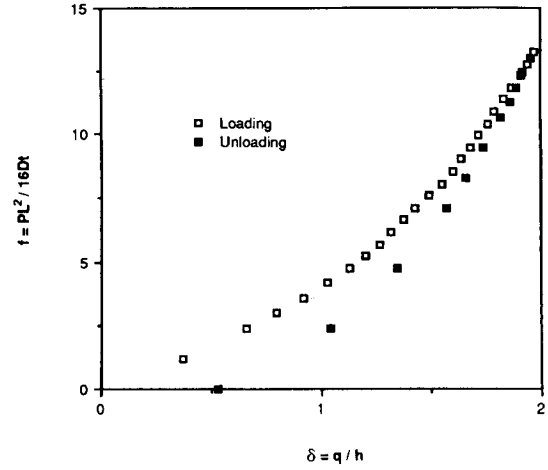

Fig. 12 Load versus punch displacement

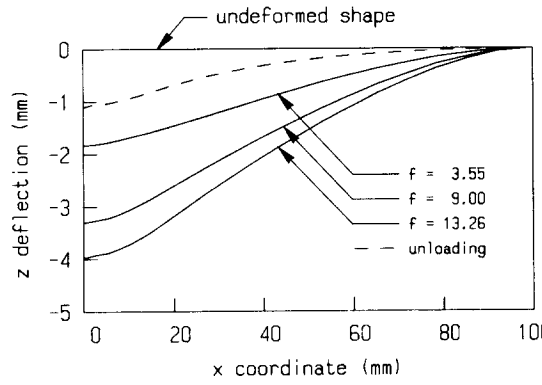

Fig. 13 Deformed shapes of plate

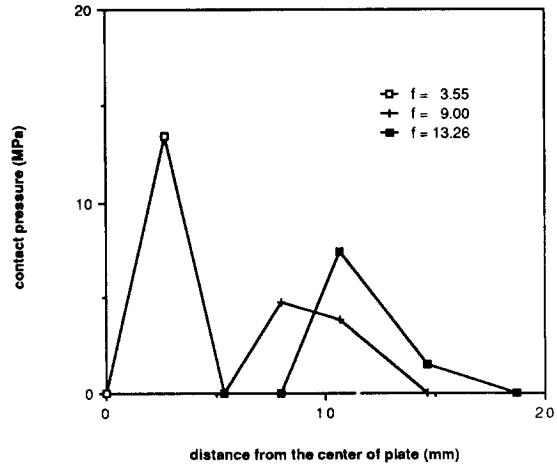

Fig. 14 Distribution of contact pressure for plate

width $L=200$mm and thickness $t=2$mm has material properties of $E=70.56$GPa and $\nu=0.33$. The workhardening characteristic of the material is expressed by the relation $\bar{\sigma}=135+186(\bar{\varepsilon}^p)^{0.38}$(MPa) where $\bar{\sigma}$ and $\bar{\varepsilon}^p$ represent the effective stress and the effective plastic strain, respectively.

Figure 12 shows the punch load versus displacement relations. As before, two nondimensional parameters, $f=PL^2/16Dt$ and $\delta=q/h$, are also employed, where the plate bending rigidity $D=Et^3/12(1-\nu^2)$. The loading is continued until f reaches 13.26, which is arbitrarily selected. The load is then removed entirely. The punch displacement recovers as much as 73%. The yielding has commenced at $f=1.77$ for the lower surface and at $f=2.37$ for the upper surface.

Figure 13 shows the deformed shapes of the mid-surface of

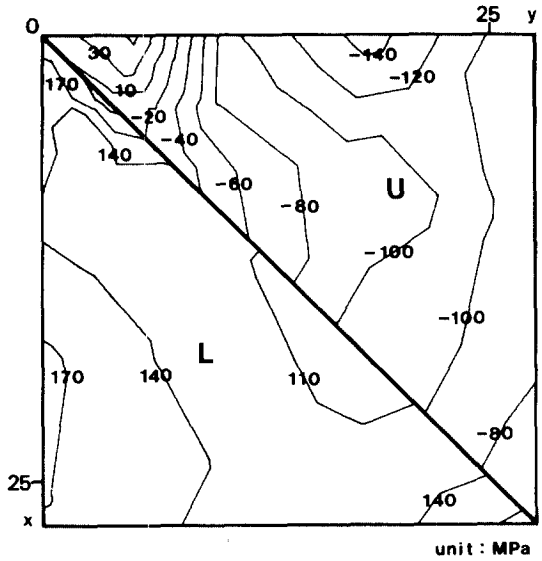

(a) $f=13.26$

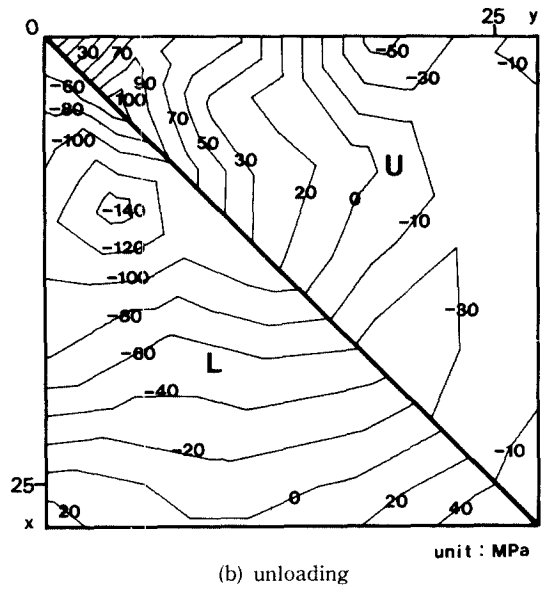

(b) unloading

Fig. 15 Stress contours of σ_x near the center

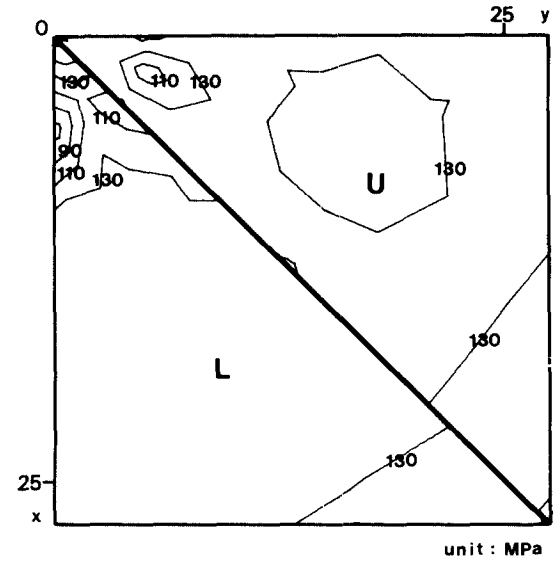

(a) $f=13.26$

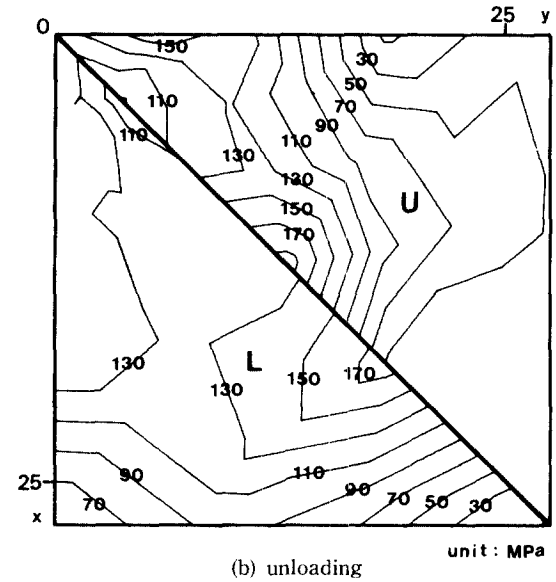

(b) unloading

Fig. 16 Stress contours of $\bar{\sigma}$ near the cener

the plate for various load levels. The radius of curvature of the deformed shape becomes smaller as the increase of loading. This means that the contact region moves. That is, the previously contacted points are gradually separated and the plate comes into contact with the punch at new contact check points as the load increases. This phenomenon is also shown in Fig. 14, where the distributions of contact pressure are displayed.

Figure 15 and 16 display the stress contours of σ_x and $\bar{\sigma}$ on the lower and upper surfaces near the center of plate at the maximum loading, $f=13.26$ and the unloading. In these figures L and U represent the lower surface and the upper surface, respectively. Compression on the upper surface and tension on the lower surface occur during loading. Upon removal of loads, compressive residual stress is seen on the lower surface and tensile on the upper surface. During loading the yielding takes place in some scattered region near the contact zone. The plastic zone moves as load changes.

6. CONCLUSIONS

In the present paper a solution method for the analysis of generally nonlinear shell contact problems has been developed through the implementation of the finite element technique and the mathematical programming method. The results of two numerical examples show that the present solution method can be efficiently applied for the analysis of those shell contact problems.

The friction on the contact surface and the change of thickness of the shell are not included in the present study, although necessary for a more elaborate modeling. The algorithm must also be extended to handle structural behaviors at or after bifurcation or global buckling in shell contact problems. These are not yet well developed and require an extensive study.

REFERENCES

Bathe, K.J. and Bolourchi, S., 1980, "A Geometric and Material Nonlinear Plate and Shell Element", Comp. Struct., Vol. 11, pp. 23~48.

Bathe, K.J., 1982, Finite Element Procedures in Engineering Analysis, Prentice-Hall, Englewood Cliffs.

Chaudhary, A. and Bathe, K.J., 1986, "A Solution Method for Static and Dynamic Analysis of Three-Dimensional Contact Problems with Friction", Comp. Struct., Vol. 24, pp. 855~873.

Cheng, J.H. and Kikuchi, N., 1985, "An Analysis of Metal Forming Processes Using Large Deformation Elastic-Plastic Formulations", Comp. Meth. Appl. Mech. Engng., Vol. 49, pp. 71~108.

Fung, Y.C., 1965, Foundations of Solid Mechanics, Prentice-Hall, Englewood Cliffs.

Haug, E.J. and Kwak, B.M., 1978, "Contact Stress Minimization by Contour Design", Int. J. Num. Meth. Engng., Vol. 12, pp. 917~930.

Hibbitt, H.D. et al., 1988, ABAQUS User's Manual Version 4.7, HKS Inc., Providence.

Hung, N.D. and de Saxce, G., 1980, "Frictionless Contact of Elastic Bodies by Finite Element Method and Mathematical Programming Technique", Comp. Struct., Vol. 11, pp. 55~67.

Joo, J.W. and Kwak, B.M., 1986, "Analysis and Applications of Elasto-Plastic Contact Problems Considering Large Deformation", Comp. Struct., Vol. 24, pp. 953~961.

Kwak, B.M., 1989, "Complementarity Problem Formulaiton and Implementation of Three-Dimensional Frictional Contact", to appear in J. Applied Mechanics, Trans. ASME.

Kikuchi, N. and Skalski, K., 1981, "An Elasto-Plastic Rigid Punch Problem Using Variational Inequalities", Arch. Mech., Vol. 33, pp. 865~877.

Lee, G.B., 1988, "Contact Analysis of Beam and Shell Structures with Geometric and Material Nonlinearities", Ph. D. Dissertation, KAIST, Seoul.

Lee, G.B. and Kwak, B.M., 1989, "Formulation and Implementation of Beam Contact Problems under Large Displacement by a Mathematical Programming", Comp. Struct., Vol. 31, pp. 365~376.

Nagtegaal, J.C. and de Jong, J.E., 1981, "Some Computational Aspects of Elastic-Plastic Large Strain Analysis", Int. J. Num. Meth. Engng., Vol. 17, pp. 15~41.

Oden, J.T. and Pires, E.B., 1984, "Algorithms and Numerical Results for Finite Element Approximations of Contact Problems with Non-Classical Friction Laws", Comp. Struct., Vol. 19, pp. 137~147.

Panagiotopoulos, P.D., 1985, Inequality Problems in Mechanics and Applications, Birkhaeuser, Boston.

Tielking J.T. and Schapery, R.A., 1981, "A Method for Shell Contact Analysis", Comp. Meth. Appl. Mech. Engng., Vol. 26, pp. 181~195.

Updike, D.P. and Kalnins, A., 1972, "Contact Pressure Between an Elastic Spherical Shell and a Rigid Plate", J. Appl. Mech., Trans. ASME, Vol. 39, pp. 1110~1114.

Yamada, Y., Yoshimura, N., and Sakurai, T., 1967, "Plastic Stress Strain Matrix and Its Application for the Solution of Elasto-Pastic Problems by the Finite Element Method", Int. J. Mech. Sci. 10, 343~354.

APPENDIX

Derviation of Matrices A and M, and Vector d For the Plate Stretched by a Rigid Punch

Denoting the rigid punch as body 1, we can write the geometry of potential contact surface of body 1 at time t as

$$g(x, y, z)=(x-x_c)^2+(y-y_c)^2 +(z-z_c)^2-R^2=0 \tag{A1}$$

where the center coordinate of the punch at time t is represented as (x_c, y_c, z_c). Using the relation

$$(u_k^2-U_k^1)\,\dot{g}_k(a_i)=2u(\tilde{x}-x_c) +2v(\tilde{y}-y_c)+2(w-q)(\tilde{z}-z_c) \tag{A2}$$

we can obtain the condition equivalent to Eq.(17)

$$\begin{aligned}&(x-x_c)^2+(y-y_c)^2+(z-z_c)^2-R^2\\&+2u(\tilde{x}-x_c)+2v(\tilde{y}-y_c)\\&+2(w-q)(\tilde{z}-z_c)\geq 0\end{aligned} \tag{A3}$$

where $(\tilde{x}, \tilde{y}, \tilde{z})$ represents the coordinates of the potential contact check points on the upper side of the plate at time t, and (u, v, w) the components of the displacment change of the points in the (x, y, z) direction. The downward motion of the punch taken as the rigid body degree of freedom is denoted as q in this equation.

Both sides of Eq.(A3) is multiplied by 1/2R to take the normalized form

$$\begin{aligned}&\frac{(\tilde{x}-x_c)^2+(\tilde{y}-y_c)^2+(\tilde{z}-z_c)^2-R^2}{2R}\\&+\frac{\tilde{x}-x_c}{R}u+\frac{\tilde{y}-y_c}{R}v+\frac{\tilde{z}-z_c}{R}(w-q)\geq 0\end{aligned} \tag{A4}$$

Now the matrices M and A, and vector d for a check point are defined as

$$\begin{aligned}M&=\left[\cdots-\frac{\tilde{x}-x_c}{R}\;-\frac{\tilde{y}-y_c}{R}\;-\frac{\tilde{z}-z_c}{R}\cdots\right]\\A&=\left[\cdots\frac{\tilde{z}-z_c}{R}\cdots\right]\\d&=\left[\cdots\frac{(\tilde{x}-x_c)^2+(\tilde{y}-y_c)^2+(\tilde{z}-z_c)^2-R^2}{2R}\cdots\right]\end{aligned} \tag{A5}$$